WEST-EAST HIGH SPEED FLOW FIELD CONFERENCE
19-22, November 2007
Moscow, Russia

NUMERICAL SIMULATION OF THE CONTINUOUS ROTATING HYDROGEN-OXYGEN DETONATION WITH A DETAILED CHEMICAL MECHANISM

Dmitry M. Davidenko*, Iskender Gökalp* and Alexey N. Kudryavtsev**

**Institut de Combustion, Aérothermique, Réactivité et Environnement,*
CNRS UPR 3021, Orléans 45071, France
davidenko@cnrs-orleans.fr, gokalp@cnrs-orleans.fr
***Khristianovich Institute of Theoretical and Applied Mechanics,*
Russian Academy of Sciences, Novosibirsk 630090, Russia
alex@itam.nsc.ru

Key words: chemically reacting flows, detonation engine performance, annular combustion chamber.

Abstract. Numerical simulations of a transverse detonation wave continuously rotating in an annular combustion chamber are performed. The investigation is aimed at a better understanding of the processes in the continuously operating detonation wave rocket engine fed with stoichiometric hydrogen-oxygen mixture. The two-dimensional Euler equations for chemically reacting flow are solved using a high-order weighted essentially non-oscillatory scheme coupled with a semi-implicit Runge-Kutta time integration method. Finite-rate chemistry is described by a kinetic model including 6 species and 7 reversible reactions. The flow structure in the combustion chamber is investigated and the dependence of main flow characteristics and combustion chamber performance on the injection total pressure, chamber length and azimuthal period is studied.

1. INTRODUCTION

Very high energy release rate, which can be achieved in detonations, for many years attracts attention of scientists and engineers to possible practical application of this phenomenon. As was shown for the first time by Ya. B. Zel'dovich [1], the detonation regime of combustion is also more efficient thermodynamically than the deflagration under the same initial conditions. One can hope that development of detonation-based fuel-burning devices will eventually lead to the design of more cost-effective and compact engines for sub-orbital spacecraft and other high-speed vehicles.

In recent years, significant efforts were undertaken for a detailed research on the concept of Pulse Detonation Engine (PDE), a device which creates propulsion by burning the fuel in a combustion chamber where a traveling detonation wave is periodically initiated [2]. Nevertheless, it seems that, owing to the difficulties of fast exhaust of the combustion products and recharging of the combustion chamber with

fresh combustible mixture, the current generation PDEs are not yet capable of running at high frequencies needed for satisfactory efficiency.

There are a few alternative concepts of detonation-based engines [3]. In particular, a promising idea that can be traced back to the work of B. V. Voitsekhovskii [4] is to use one or more detonation waves spinning in an annular tube, which is constantly refilled by a combustible mixture from one end. It is the so-called Continuous Detonation Wave Engine (CDWE). The main advantages of CDWE are the continuous operation and a high combustion rate. Its feasibility has been experimentally proven for the first time at the Lavrent'yev Institute of Hydrodynamics (Novosibirsk, Russia). In many aspects, CDWE is close to PDE operating at very high frequency (several kHz). For a review of this concept, a detailed description of its experimental investigations, and comparison with PDE and conventional rocket engine, one can refer to the recent publications [5,6].

Numerical simulations can contribute significantly to the study and better understanding of the CDWE internal process. However, in contrast to PDE, very few attempts to perform numerical simulation of the CDWE operation were undertaken [7,8].

In the present work, the detonation wave propagation in CDWE is simulated numerically by solving the Euler equations for a chemically reacting flow. A detailed chemical model (6 species, 7 reactions) is used to describe the combustion of stoichiometric hydrogen-oxygen mixture. The governing equations are solved with a high-resolution shock-capturing WENO (weighted essentially non-oscillatory) scheme. The numerical simulations are used to obtain a clear picture of processes in the combustion chamber of CDWE, elucidate the underlying physical mechanisms, and investigate the influence of different parameters (such as injection characteristics and geometric sizes) on the phenomena in the combustion chamber and its performance.

2. PROBLEM FORMULATION, GOVERNING EQUATIONS, AND NUMERICAL APPROACH

2.1. Problem formulation

A typical combustion chamber of CDWE is schematically shown in Fig. 1. It is an annular cylindrical tube with one closed and another open ends. The mixture of fuel and oxidizer (1) is injected from the closed end (2) through a ring slit or a large number of regularly arranged small holes.

Depending on the conditions of initiation, the transverse detonation waves (3) travel azimuthally in the clockwise or counter-clockwise direction. They burn the layer of combustible gas (4), which is restored during the time period between successive detonation fronts. For a stable detonation propagation, the thickness of the fresh mixture layer h must be about 10-20 mm and the spatial period l between the fronts is typically $(7\pm2)\ h$ depending on the injection conditions [6]. The detonation wave propagation induces oblique shock waves (5) in the combustion products. The combustion products flow towards the duct open end (6) and then discharge from the chamber through a divergent nozzle (not shown in the scheme). Due to the detonation products expansion, a supersonic flow velocity can be achieved though the device has no geometrical throat.

It should be noted that the numerical simulation of CDWE in the full 3D configuration can be too expensive. It is particularly true in the case of a parametric study. The problem can be simplified by assuming that the gap between the duct walls is small in comparison with its radius and the flow variations in the radial direction are

negligible. Thus the computations are performed in a 2D rectangular domain with the periodical boundary conditions imposed along one coordinate direction.

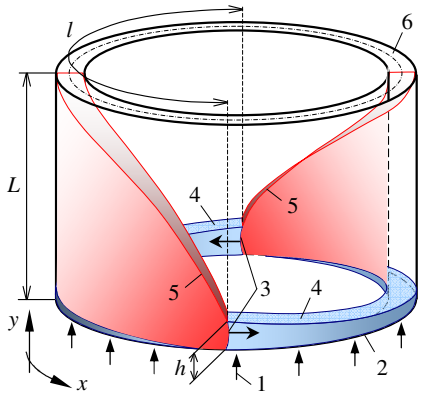

Fig.1. Schematic of CDWE combustion chamber.

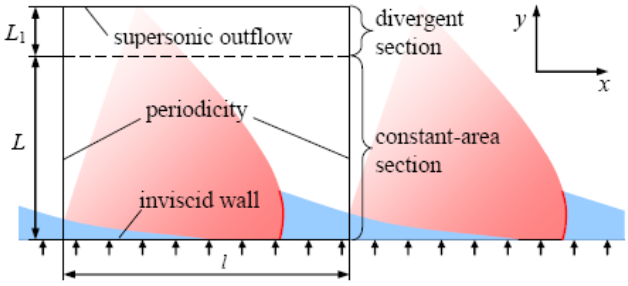

Fig.2. Computational domain for CDWE simulation

The size of the computational domain along x (the periodicity length) is denoted thereafter as l. Along y, the domain consists of a constant-area and a divergent sections whose lengths are denoted by L and L_1. In the present parametric study, the domain dimensions vary within the following ranges: l = 50-100 mm, L = 10-100 mm. Within the divergent section of the duct ($L < y < L+L_1$), it is assumed that the duct cross-section area A linearly increases with y. The divergent section length L_1 = 10-20 mm and area ratio $A(L+L_1) / A(L)$ = 1.5-2 are arbitrarily chosen with the only purpose to ensure the supersonic outflow all along the upper boundary ($y = L+L_1$). Hence the combustion chamber operation does not depend on the external conditions.

The injection of stoichiometric mixture of H_2 and O_2 through the lower boundary ($y = 0$) is modeled as follows. The specified injection parameters are: the net area of injector throats A_j normalized by the overall area A_w of the injection wall, $A_j / A_w = 0.1331$, the stagnation pressure $P_{t\,j}$ = 1-6 MPa, and stagnation temperature $T_{t\,j}$ = 300 K. The area-specific mass flow rate $g_j(x) = G_j(x) / A_w$ depends on the wall pressure distribution $P_w(x)$. We suppose that the mixture is injected through an infinitely large number of uniformly distributed injectors so that g_j varies from zero at $P_w \geq P_{t\,j}$ to $g_{j\,max}$ at $P_w \leq P_{cr\,j}$, where $P_{cr\,j}$ is the pressure at which the sonic injection condition is achieved.

2.2. Governing equations

Viscosity, heat conductivity, and diffusion effects are neglected in the present investigation so that the flow is governed by the 2D Euler equations for a mixture of thermally perfect gases. Standard thermodynamic data [9] are approximated by piece-wise linear functions for the species specific heats $C_P(T)$ and piece-wise quadratic functions for the species enthalpies $H(T)$. This kind of approximation is found to be precise and considerably less time consuming than the standard polynomial functions.

The chemical kinetic mechanism, which was previously applied to supersonic combustion computations [10], is adopted here to calculate the chemical source terms. This mechanism includes 6 species, H_2, O_2, H_2O, H, O, and OH, and 7 reversible

chemical reactions. The rate constants of the backward reactions have been refitted in a larger temperature range suitable for detonation simulations.

2.3. Numerical approach

A high-resolution Euler code for a multispecies flow is based on the shock-capturing, weighted essentially non-oscillatory (WENO) scheme of the fifth order [11] extended to chemically reacting flows. In contrast with more wide-spread total variation diminishing (TVD) schemes, the WENO schemes do not decrease their accuracy down to the first order near smooth extrema of the solution. Thus, they add to the solution a significantly smaller amount of numerical diffusion and allow one to improve noticeably the flowfield resolution.

To avoid restrictions on the time step, which are resulted from the stiff chemical source terms and can be prohibitively severe at high pressures, the time integration is performed with the semi-implicit additive Runge-Kutta scheme ASIRK2C [12]. The convective terms are included in the explicit operator whereas all the source terms are treated implicitly. The time step is controlled by the Courant number that is close to 0.5-0.7. The influence of spatial and temporal resolution on the simulation results is analyzed below. The code is parallelized using the MPI library.

Perfectly reflecting or inviscid wall boundary conditions are imposed along the lower boundary. The mass, momentum and energy fluxes due to injection are evaluated every time step according to the local pressure in the first row of grid cells next to the wall. These fluxes are then added to the numerical fluxes calculated by the Euler solver in the first cell row. The effect of duct expansion is modeled by introducing geometrical source terms into the governing equations. A simple extrapolation of conserved variables is utilized on the upper boundary.

3. CODE VALIDAION AND GRID RESOLUTION STUDIES

3.1. Ignition delay time and ZND solution

The thermochemical model and numerical code have been validated for some simple test problems. First, simulations of the 0D constant-volume autoignition of a stoichiometric H_2-O_2 mixture diluted by Ar (H_2:O_2:Ar = 0.1:0.05:99.85) were conducted for the following initial conditions: T_{ini} = 1360-1880 K and P_{ini} = 6.48 MPa. The results on the ignition delay time t_{ign}, obtained with the present mechanism and two other mechanisms [13, 14] are compared with shock-tube experimental data [15] in Fig. 3. A good agreement between the experiment and numerical predictions is observed within the temperature range corresponding to the detonation conditions ($1000/T_{ini}$ = 0.55-0.56).

Using a Zel'dovich-von Neumann-Döring (ZND) model [16] with the three kinetic mechanisms, 1D solutions have been obtained for Chapman-Jouguet (CJ) detonations under the following conditions ahead of the detonation front: H_2:O_2 = 66.7:33.3, T_∞ = 300 K, P_∞ = 0.05-1 MPa. Figure 4 shows the dependence of the ignition delay distance x_{ign} and the temperature T_{sh} just behind the shock front on P_∞. One can conclude that the most significant divergence of x_{ign} is observed at high pressure when the present model underestimates the ignition delay.

3.2. Resolution studies for a propagating detonation wave

Typically, the detonation wave engine operates at high pressure when the ignition delay

distance is small and cannot be resolved in 2D numerical simulation of full-scale chamber without using extremely fine grids. Even if the internal structure of the detonation front is unresolved, the numerical solution must correctly predict the main detonation characteristics such as the propagation velocity and CJ conditions. The influence of the spatial and temporal resolution on the detonation velocity has been investigated by simulating 1D freely propagating detonations at P_∞ = 0.1 MPa, 0.35 MPa, and 0.7 MPa. The mixture composition and T_∞ are the same as for the ZND simulations. For the case P_∞ = 0.35 MPa, Fig. 5 shows the variations of the detonation wave velocity D with the time step Δt for different spatial grid steps Δx. Results obtained on the coarser grids (Δx = 0.05 mm and 0.1 mm) depend on both Δt and Δx. The converged result, achieved with $\Delta x \le 0.025$ mm, corresponds exactly to the CJ velocity D_{CJ} = 2904 m/s. For P_∞ = 0.1 MPa and 0.7 MPa, the allowable grid step is respectively 0.1 mm and 0.01 mm.

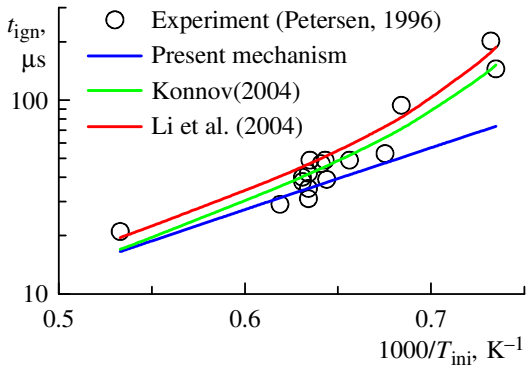

Fig. 3. Validation of the kinetic mechanism by the ignition delay time predictions for shock-tube conditions.

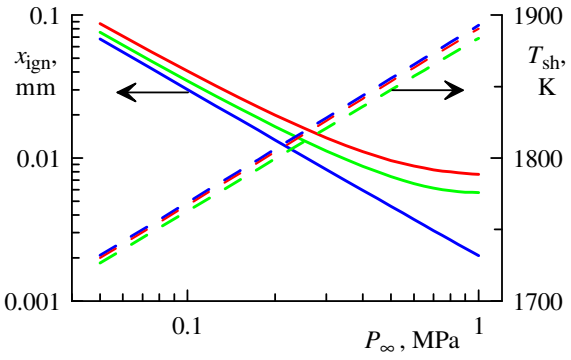

Fig. 4. Ignition distance and temperature behind the shock front in the CJ detonation from ZND model. Line colors correspond to the same mechanisms as in Fig. 2.

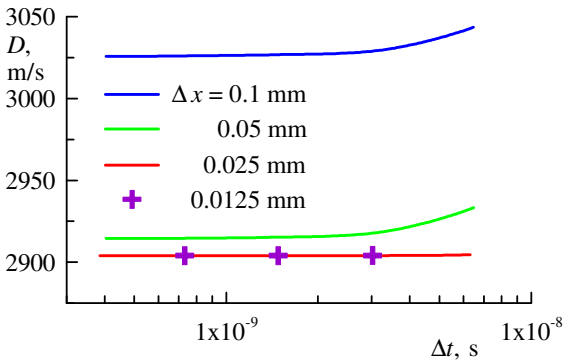

Fig. 5. Dependence of the detonation wave velocity on the time step and spatial resolution for P_∞ = 0.35 MPa.

It is worth of noting that development of 1D pulsating instability was observed in the computations with much finer grids ($\Delta x \le 1$ μm). 2D simulations for lower initial

pressures, when x_{ign} increases significantly, demonstrate also the development of transverse disturbances and formation of cellular detonation waves.

3.3. Resolution in CDWE simulations

For numerical simulation of CDWE operation, a 2D computational mesh is constructed of parallel horizontal and vertical lines. Along y, the mesh has a uniform step $\Delta y = 0.05$ mm near the lower boundary, within a layer slightly larger than the detonation wave height. Then Δy is stretched gradually towards the upper boundary. The number of cells in the y-wise direction varies from 250 to 560 depending on L.

The simulations can be performed both in the laboratory frame of reference where the detonation wave rotates continuously and in the reference frame moving with the detonation wave. The first case requires either a uniform mesh in the x-wise direction, which becomes too large when the pressure is high, or a dynamically adapted mesh that is not yet available with the present code. In the moving reference frame, the detonation wave takes a fixed position with respect to the computational mesh whose x-wise step can be easily refined in the vicinity of the detonation front. The two techniques were utilized in the present study. At the lowest injection mass flow rate ($P_{tj} = 1$ MPa), the simulation was made in the laboratory frame using a mesh with a constant step $\Delta x = 0.1$ mm (1000 cells per horizontal row). For the other mass flow rates, preliminary solutions were obtained in the laboratory frame and the final ones were computed in the moving frame on refined meshes. In the latter case, Δx has a minimum value of 0.025 mm or 0.01 mm, respectively for $P_{tj} = 3$ MPa and 6 MPa, and a maximum value of 0.2 mm. The number of cells in the x-wise direction varies from 500 to 900 depending on l and Δx_{min}. This choice of Δx_{min} provides that the detonation propagation is correctly simulated however the detonation internal structure is unresolved. In view of this, the error in the ignition delay due to the chemical model is unimportant.

A particular problem has been encountered with the numerical treatment of the contact boundary between the fresh mixture layer and combustion products. Even though the flow is considered inviscid, the numerical scheme introduces some artificial diffusion that results in a "pseudolaminar" flame along that boundary. The flame propagation velocity depends on the spatial resolution and local conditions. It is high enough to burn up to 10-20 % of mixture before the detonation wave arrives. Even if a similar effect is observed in the experiment [6, 7], we prefer not to simulate it without a suitable diffusion model. To avoid this problem, the chemical source terms on the contact boundary were artificially suppressed. With this modification, the difference between the injected mass and that burnt in the detonation wave does not exceed 0.1%.

From the considerations presented in this section, we can state that the present computational approach is not suitable for predicting the limits of the detonation propagation because the internal detonation wave structure is not accurately resolved. Hence our study is focused on the regimes of stable propagation of detonation. We do not analyze in detail the detonation initiation and transition to a stable propagation

4. RESULTS OF CDWE SIMULATIONS

4.1. Flow structure in the combustion chamber of CDWE

It is assumed that at the initial time moment the chamber is filled by the combustion products except a triangular region of fresh mixture near the injection boundary; a high-

temperature and high-pressure spot is placed within that triangular region to initiate the detonation. After the detonation initiation, several tens of periods of detonation rotation are needed to reach a stable regime when the entire flowfield becomes globally steady in the moving frame of reference. To reduce the computational time, we used whenever possible previous solutions to initialize a new computational case.

Here we present numerical results on the CDWE combustion chamber obtained for various injection pressures P_{tj} and geometrical sizes L and l. Before analyzing the effect of each parameter, we consider in detail a single case corresponding to the following parameter set: $P_{tj} = 3$ MPa, $L = l = 100$ mm. Except few details specially mentioned below, the other simulated flowfields are very similar.

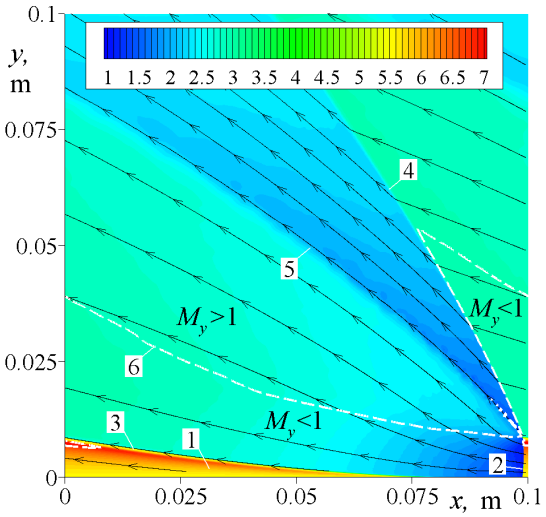

Fig. 6. Flowfield structure in the combustion chamber: $P_{tj} = 3$ MPa, $L = l = 100$ mm. The colored band indicates the scale of Mach number M_D in the moving reference frame

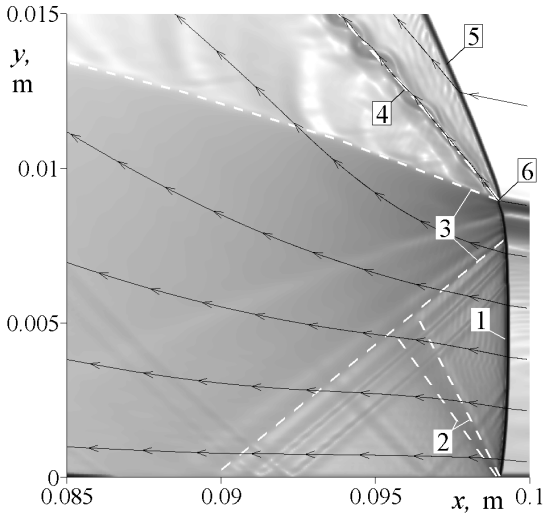

Fig. 7. Flowfield structure around the detonation wave. Schlieren-like representation of density gradient in an arbitrary exponential scale.

The general flowfield structure within the constant-area section is shown in Fig. 6. The colored field displays the variation of the Mach number M_D in the moving reference frame along with superimposed streamlines. Several characteristic zones are clearly depicted. The fresh mixture layer (1) is continuously growing from the lower boundary. In this layer, M_D is very high, from 5.5 up to 7. The detonation wave (2) is situated close to the right boundary. In front of the detonation wave, the mean static pressure and temperature are respectively 0.34 MPa and 259 K. The velocity of detonation propagation in the laboratory frame of reference, U_D, is of 2889 m/s, and the mean velocity of the detonation front with respect to the fresh mixture, D, is of 2922 m/s. Under these particular conditions, the propagation velocity of the ideal CJ detonation is $D_{CJ} = 2915$ m/s that is the simulated detonation is well matched the CJ regime. The maximum pressure and temperature obtained in the detonation wave are respectively 9.5 MPa and 4090 K.

Behind the detonation wave, the flow is subsonic within a very narrow zone. It rapidly accelerates to supersonic speeds due to a strong expansion of combustion products, which is clearly indicated by the divergent streamlines. The injection is

suppressed over some distance behind the detonation wave because of a high pressure there. Two other waves are visible in Fig. 6 that originate from the point where the detonation wave meets the boundary (3) of the fresh mixture layer: a shock wave (4), which recompresses the flow of combustion products produced by the previous detonation, and a slip line or contact discontinuity (5), which separates the two streams of combustion products. A white dashed line (6) delimits the flowfield zones where the vertical velocity component is subsonic ($M_y < 1$) or supersonic ($M_y > 1$). One can notice that at $y > 50$ mm the flow is fully supersonic in the y-wise direction. In this case the duct expansion is not necessary to obtain a supersonic flow at the combustion chamber exit. The observed flow structure is qualitatively similar to that described in [6, 7, 8].

A closer view of the region around the detonation wave is shown in Fig. 7. It gives a schlieren-like representation of the computed field of density gradient. The main flowfield features are highlighted by white lines. The maximum height of the fresh mixture layer h is 8.9 mm. In this layer, the velocity vector angle with respect to the wall varies from 5° to 9°. The detonation wave front (1) is slightly curved. It is practically normal to the mixture stream near the wall and becomes oblique as the velocity vector angle increases. Immediately behind the detonation wave, the velocity vector angle varies from 3° to 16°. There are two expansion fans at each end of the detonation front. A weak fan (2) is originated from the point where the detonation front meets the wall. It turns the streamlines towards the wall. A strong fan (3) emanates from the triple point at the top of the detonation front. This fan turns the stream upwards and aligns it with the deflected contact boundary (slip line) (4). The shock wave (5) originating from the triple point (6) is oblique. When the flow passes the shock close to the triple point, its Mach number falls from 2.95 to about 1.4-1.5. The shear between the two flows separated by the slip line is strong as the velocity difference is about 1000 m/s. Nearly the same velocity difference is found over the contact boundary separating the fresh mixture and combustion products in front of the detonation wave.

4.2. Performance of CDWE

Main results characterizing the combustion chamber performance are summarized in Table 1 for all the simulated cases. The quantities that are not yet introduced have the following definitions:

– average specific mass flow rate

$$\overline{g}_{\mathrm{j}} = \frac{1}{l}\int_0^l \rho_{\mathrm{j}}\, v_{\mathrm{j}}\, \mathrm{d}\, x$$

where ρ_{j} is the density and v_{j} is the y-wise velocity component of injected mixture;

– frequency of the detonation rotation

$$f_D = U_D / l$$

– average wall pressure

$$\overline{P}_{\mathrm{w}} = \frac{1}{l}\int_0^l P_{\mathrm{w}}\, \mathrm{d}\, x$$

– combustion chamber specific impulse

$$I_{\mathrm{sp}} = \frac{1}{\overline{g}_{\mathrm{j}}\, l}\int_0^l (\rho\, v^2 + P)\, \mathrm{d}\, x,$$

where ρ, v, and P are taken at $y = L$ although the y-wise momentum is globally conserved;

– relative variation of the y-wise velocity component v with respect to its mass-average value v_m at the combustion chamber exit ($y = L$)

$$\delta v(y = L) \equiv \frac{\max[v(x,\ y = L)] - \min[v(x,\ y = L)]}{v_m(y = L)},$$

$$v_m(y) = \int_0^l \rho(x, y)\, v(x, y)\, \mathrm{d}\, x \Big/ \int_0^l \rho(x, y)\, \mathrm{d}\, x$$

– variation of the angle of velocity vector with respect to the y-wise direction at the combustion chamber exit

$$\Delta\beta(y = L) = \beta_{\max}(y = L) - \beta_{\min}(y = L),$$

$$\beta = \arctan(u / v)$$

where u is the x-wise velocity component in the laboratory frame of reference. δv and $\Delta\beta$ are introduced here to characterize the nonuniformity of the velocity profile at the combustion chamber exit that can affect the nozzle performance.

Table 1. Main characteristics of the detonation propagation and combustion chamber performance.

$P_{t\,j}$ MPa	L mm	l mm	$\overline{g}_j$ kg/(s·m^2)	$\overline{g}_j / g_{j\,max}$ %	f_D kHz	U_D m/s	D, m/s	h/l %
1	100	100	173	86.2	27.9	2795	2829	9.45
3	100	100	513	85.5	28.9	2889	2922	8.88
6	100	100	1024	85.3	29.3	2933	2964	8.63
3	40	100	513	85.5	28.9	2889	2922	8.88
3	20	100	513	85.5	28.9	2889	2921	8.78
3	10	100	519	86.5	28.9	2889	2922	10.27
3	40	75	514	85.7	38.5	2886	2920	8.97
3	40	50	515	85.9	57.6	2881	2917	9.15

$P_{t\,j}$ MPa	L mm	l mm	$\overline{P}_w$ MPa	$P_{w\,min} / \overline{P}_w$	$P_{w\,max} / \overline{P}_w$	I_{sp} m/s	$\delta v(y = L)$ %	$\Delta\beta(y = L)$ deg
1	100	100	0.434	0.320	6.79	2699	39.6	31.0
3	100	100	1.323	0.314	7.12	2765	40.2	31.9
6	100	100	2.668	0.320	6.91	2794	41.0	32.2
3	40	100	1.323	0.316	7.29	2760	49.5	56.3
3	20	100	1.323	0.314	7.11	2759	57.5	72.5
3	10	100	1.273	0.326	5.93	2631	65.2	99.6
3	40	75	1.323	0.314	7.20	2756	46.3	48.1
3	40	50	1.324	0.314	7.17	2749	40.4	36.9

4.3. Influence of geometrical and injection parameters of CDWE The effect of the injection pressure $P_{t\,j}$ has been studied for fixed dimensions $L = l = 100$ mm. The choice of $P_{t\,j}$ provides that the specific mass flow rate $\overline{g}_j$ corresponds to the experimental conditions [6] at $P_{t\,j} =$ 1 MPa, whereas it is within the range of CDWE operating conditions [5] at $P_{t\,j} =$ 3-6 MPa. By analyzing the data from Table 1, one can find that $\overline{g}_j$, $\overline{P}_w$, $P_{w\,min}$, and $P_{w\,max}$

are linear increasing functions of P_{tj}. The dependencies $\overline{P}_w(P_{tj})$ and $\overline{g}_j(P_{tj})$ are shown in Fig. 8. The other characteristics are quite conservative with respect to P_{tj} : the overall growth in frequency f_D and detonation velocity U_D is about 5 %. Even if $\overline{g}_j$ is continuously growing, the maximum height h of the mixture layer decreases globally by 9 % because of the simultaneous rise of P_w and f_D. The overall increase in the specific impulse I_{sp} is about 3.5 %. The nonuniformity of the velocity profile remains practically unchanged.

To investigate the influence of the dimensions L and l, P_{tj} is fixed at 3 MPa. The value of L is taken equal to 40 mm, 20 mm, and 10 mm at constant l = 100 mm. The detonation propagation is insensible to the variation of L even if L is close to h. When $L \le 40$ mm, the flow is not entirely supersonic at $y = L$. The subsonic-supersonic transition occurs at the very beginning of the divergent section. At L = 10 mm, P_w slightly diminishes and the top of the mixture layer appears in the divergent section ($h > L$). The detonation wave remains stable however I_{sp} globally decreases by 4.9 %. At the same time, the velocity profile nonuniformity strongly increases.

Finally, the azimuthal period l is reduced to 75 mm and 50 mm keeping the other dimension constant L = 40 mm. From the data given in Table 1, one can conclude that the frequency f_D and mixture layer height h are inversely proportional to l. The other quantities related to the injection, detonation propagation, and wall pressure distribution have no any noticeable change. Instantaneous distributions of wall pressure obtained for the three different periods are plotted in Fig. 9. If the x-coordinate is normalized by l, the three curves become coincident. We also verified that the entire flowfield is self-similar if both the coordinates are normalized by l. Contrary to the reduction of L, a smaller period results in more homogeneous velocity profile at the combustion chamber exit.

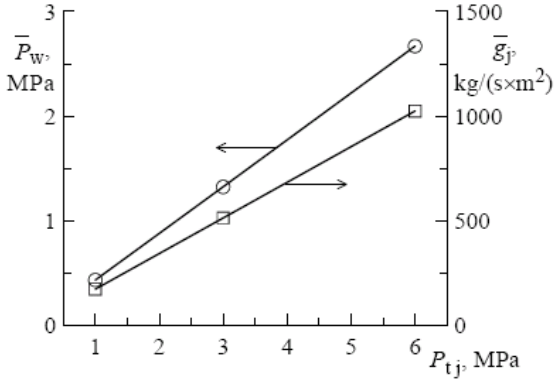

Fig. 8. Average wall pressure and specific mass flow rate as functions of the injection total pressure.

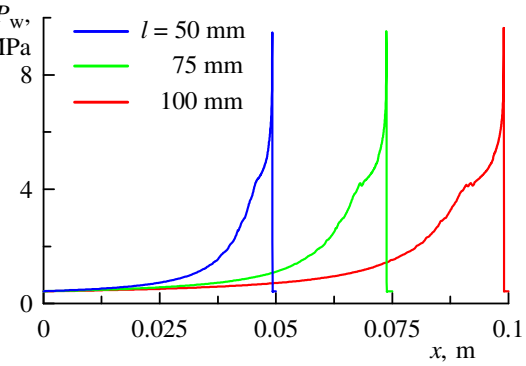

Fig. 9. Instantaneous distributions of wall pressure for different azimuthal periods.

As compared to the present results, the experiment [6] and simulations by Zhdan et al. [8] give lower detonation speeds. The experimentally observed deficit in U_D is certainly due to imperfect mixture (separate injection of fuel and oxidizer, dilution with combustion products) and viscous losses. The models applied by Zhdan et al. are probably tuned to match the experimental velocity however their general assumptions are the same as we adopted here for the problem formulation.

5. CONCLUSIONS

Numerical simulations of continuous rotating detonation in the stoichiometric hydrogen/oxygen mixture have been performed using high-resolution numerical schemes and a detailed thermochemical model. Even if the present approach is rather idealized, it allowed us to investigate the flowfield structure and study the effects of the injection pressure and combustion chamber geometry on the detonation propagation and combustion chamber performance.

In future we plan to complete this study by an investigation of the internal detonation wave structure and stability of detonation propagation in a layer of combustible mixture as well as by an evaluation of the CDWE performance accounting for the flow expansion in the nozzle.

ACKNOWLEDGEMENTS

The present work was supported by MBDA France. Special thanks to Dr. E. Daniau for very helpful discussions. The computations resources were provided by the EPEE Federation of CNRS and University of Orléans.

REFERENCES

[1] Ya.B. Zel'dovich, "On the use of detonative combustion in power engineering", *J. Techn. Phys.*, 10, 1453-1461 (1940), (in Russian).

[2] G.D. Roy, S.M. Frolov, A.A. Borisov, and D.W. Netzer, "Pulse detonation propulsion: challenges, current status, and future perspective", *Progress in Energy and Comb. Sci.*, 30, 545-672 (2004).

[3] K. Kailasanath, "Review of propulsion applications of detonation waves", *AIAA Journal*, 38, 1698-1708 (2000).

[4] B.V. Voitsekhovskii, "Stationary spin detonation", *J. Appl. Mech. Techn. Phys*., 3, 157-164 (1960) (in Russian).

[5] E. Daniau, F. Falempin, and S. Zhdan, "Pulsed and rotating detonation propulsion systems: first step toward operational engines", *AIAA Paper* 2005-3233 (2005).

[6] F.A. Bykovskii, S.A. Zhdan, and E.F. Vedernikov, "Continuous spin detonations", *J. Propulsion and Power*, 22, 1204-1216 (2006).

[7] S.A. Zhdan, A.M. Mardashev, and V.V. Mitrofanov, "Calculation of the flow of spin detonation in an annular chamber", *Combust. Explosion and Shock Waves*, 26, 210-214 (1990).

[8] S.A. Zhdan, F.A. Bykovskii, and E.F. Vedernikov, "Mathematical modeling of a rotating detonation wave in a hydrogen-oxygen mixture", *Combust. Explosion and Shock Waves*, 43, 449-459 (2007).

[9] A. Burcat and B. Ruscic, "Third millennium ideal gas and condensed phase thermochemical database for combustion with updates from active thermochemical tables", *Report No. ANL-05/20, TAE 960*, Argonne National Laboratory, Technion (2005).

[10] D.M. Davidenko, I. Gökalp, E. Dufour, and P. Magre, "Systematic numerical study of the supersonic combustion in an experimental combustion chamber", *AIAA Paper* 2006-7913 (2006).

[11] G.-S. Jiang and C.-W. Shu, "Efficient implementation of weighted ENO schemes", *J. Comput. Phys*., 126, 202-228 (1996).

[12] X. Zhong, "Additive semi-implicit Runge-Kutta methods for computing high-speed nonequilibrium reactive flows. *J. Comput. Phys*., 128, 19-31 (1996).

[13] A.A. Konnov, "Refinement of the kinetic mechanism of hydrogen combustion", *Khimicheskaya Fizika*, 23, 5-18 (2004).

[14] J. Li, Z. Zhao, A. Kazakov, and F.L. Dryer, "An updated comprehensive kinetic model of hydrogen combustion", *Int. J. Chem. Kinet*., 36, 566-575 (2004).

[15] E.L. Petersen, D.F. Davidson, M. Röhrig, and H.K. Hanson, "High-pressure shock-tube measurements of ignition times in stoichiometric H_2/O_2/Ar mixtures", *Proc. 20th Int. Symp. Shock Waves*, Vol.2, 941-946 (1996).

[16] J.E. Shepherd, "The chemical kinetics of hydrogen-air-diluent detonations", *Prog. Astronaut. Aeronaut.*, 106, 263-293 (1986).